The Effect of Vertical Stability on Tornadogenesis

L. M. LESLIE

Australian Numerical Meteorology Research Centre, Melbourne, Australia 3001

R. K. SMITH

Department of Mathematics, Monash University, Clayton, Australia 3168

(Manuscript received 5 October 1977, in final form 23 January 1978)

ABSTRACT

A recent numerical study of vortex growth in a flow configuration which models the principal characteristics of a tornado cyclone (Smith and Leslie, 1978) is extended to take account of vertical stability. It is shown that for a given strength of convection and rotation (in the model, the driving effect of a 'supercell' updraft is simulated by an imposed body force), the intensity of the mature vortex which forms in the presence of a typical vertical gradient of potential temperature is significantly lower than that which forms in an adiabatic atmosphere. We conclude that the effects of vertical stratification on tornadogenesis may often be important and may prevent some vortices, which might otherwise do so, from establishing ground contact.

1. Introduction

The paucity of observational data on tornadoes has greatly hindered the development of convincing theoretical simulations of their dynamics and evolution. In recent years the National Severe Storms Laboratory (NSSL) in Oklahoma has intensified its efforts to remedy this deficiency and central to their program has been the use of Doppler radar techniques to determine the air motions in severe thunderstorms (see, e.g., Burgess, 1976; Brown and Lemon, 1976; Brandes, 1977a,b). As in other branches of meteorology, the acquisition of data calls for the simultaneous development of models; ideally, to provide a basis for interpretation of the data and/or for the design of future measurement programs, and it is in this spirit that the present study is conceived.

Three important aspects of tornadogenesis which theory must explain are the downward growth of a vortex from its parent cloud to the ground, the relative rarity of this event compared with the frequency of occurrence of apparently suitable parent thunderstorms, and the rarity compared with the frequency with which these storms spawn pendant funnel clouds. A mechanism for growth which has these attributes is described and illustrated using a simple numerical model by Smith and Leslie (1978; henceforth referred to as TG). In the model, the "supercell" updraft of a tornado cyclone is represented by an axial body force located in the central upper portion of a cylindrical flow region and rotation is included by specifying the circulation at the radial boundary of the computational domain. The calculated flow fields show how a vortex is generated aloft when the body force is "switched on" and how it develops downward, and we believe they provide an appealing explanation for the organization of thunderstorm rotation by the updraft to create a vortex. Recent Doppler radar studies of tornado-producing thunderstorms (Brown and Lemon, 1976) indicate that this occurs initially at mid-levels within the cloud and progresses downward. The calculations also confirm the prediction of Morton (1969, p. 325) that the evolution of a concentrated vortex requires the forcing strength and the level of rotation to be confined within a narrow range of values; this would explain why relatively few storms spawn tornadoes. Finally, the studies in TG suggest that for a vortex to develop down to the ground, there must either be a sufficient level of ambient rotation at lower levels initially, or the vortex circulation must induce this, and when the rotation is confined to upper levels, we are able to simulate steady suspended vortices.

A possible limitation of our model is the assumption of homogeneous, incompressible flow, since observations of static stability in the rain-cooled air at low levels ($\lesssim$440 m) in the vicinity of severe thunderstorms (Goff, 1976) show vertical gradients of potential temperature which are typically about 0.8°K (100 m)$^{-1}$ and in extreme cases about twice this value. Therefore, it is conceivable that vertical stability may be an important factor in tornado dynamics, although the extent to which it is likely to be significant in inhibiting vortex formation appears to have received

0022-4928/78/1281-1288$05.00

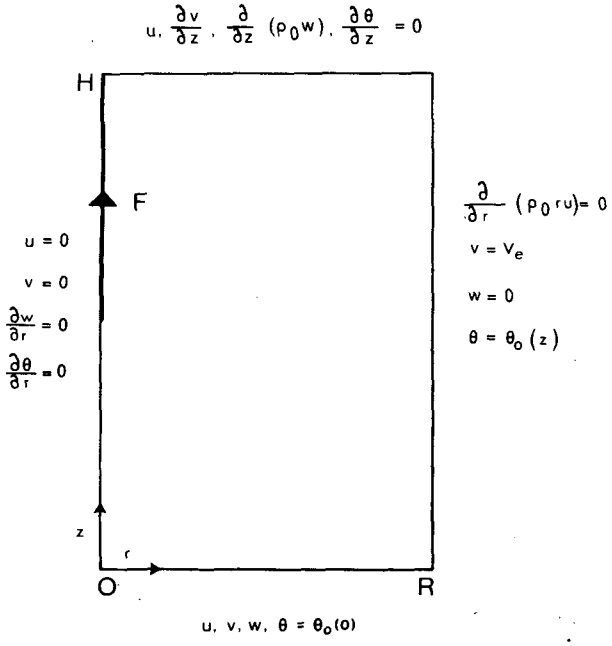

FIG. 1. Schematic representation of the flow domain together with the boundary conditions used in the calculations.

little study hitherto. In this paper the model described in TG is extended to explore this possibility.

2. The model

The flow domain over which computations are performed is a cylindrical region of air with radius R and depth H, with its axis vertical. It is bounded by a rigid (no-slip) lower boundary but air may enter or leave the region in a normal direction through the side and upper boundaries. The flow is taken to be axisymmetric and is driven by a body force imposed along the upper part of the axis and distributed over two radial grid intervals. Rotation is imposed by prescribing a swirling velocity component on air entering through the side boundary.

The equations are a more general version of the approximate set derived by Ogura and Phillips (1962) for studies of deep convection in a nearly adiabatic atmosphere. The principal approximation here is the neglect of radial and temporal variations of density in the continuity equation, thereby excluding acoustic wave disturbances. The momentum equations are unapproximated except for the usual diffusive terms representing turbulent shear stresses. The full set of equations, including the thermodynamic equation, may be written in the form

$$\frac{\partial}{\partial r}(\rho_0 ru)+\frac{\partial}{\partial z}(\rho_0 rw)=0, \tag{2.1}$$

$$\frac{Du}{Dt}-\frac{v^2}{r}=-c_p\theta\frac{\partial\pi'}{\partial r}+K_M\left(\nabla^2 u-\frac{u}{r^2}\right), \tag{2.2}$$

$$\frac{Dv}{Dt}+\frac{uv}{r}=K_M\left(\nabla^2 v-\frac{v}{r^2}\right), \tag{2.3}$$

$$\frac{Dw}{Dt}=-c_p\theta\frac{\partial\pi'}{\partial z}+F+g\frac{\theta'}{\theta_0}+K_M\nabla^2 w, \tag{2.4}$$

$$\frac{D\theta}{Dt}=K_H\nabla^2\theta, \tag{2.5}$$

where (u,v,w) are velocity components in the cylindrical coordinate system (r,ϕ,z) coaxial with the flow, $D/Dt\equiv\partial/\partial t+u\partial/\partial r+w\partial/\partial z$, t is the time, ∇^2 the Laplacian operator, θ the potential temperature, θ_0 its ambient value at height z, $\theta'=\theta-\theta_0$, $\pi=(p/1000)^\kappa$ is the Exner function, where p is the pressure (mb) and κ the adiabatic constant for dry air ($=0.286$), π' is the difference between π and its ambient value π_0 at the same height, ρ_0 is the ambient density field ($=10^5\pi_0^{(1/\kappa)-1}/\kappa c_p\theta_0$) when c_p, the specific heat of dry air at constant pressure is in SI units, K_M and K_H are the turbulent diffusivities of momentum and heat, respectively (these are assumed constant and in all but one experiment are taken to be equal) and g is the acceleration due to gravity.

The boundary conditions, also displayed in Fig. 1 are as follows:

$$\left.\begin{aligned}&\text{On } z=0\text{: } u=0,\ v=0,\ w=0,\ \theta=\theta_0(0)\\&\text{On } z=H\text{: } u=0,\ \partial v/\partial z=0,\ \partial(\rho_0 w)/\partial z=0,\ \partial\theta/\partial z=0\\&\text{On } r=0\text{: } u=0,\ v=0,\ \partial w/\partial r=0,\ \partial\theta/\partial r=0\\&\text{On } r=R\text{: } \partial(\rho_0 ru)/\partial r=0,\ v=V_e,\ w=0,\ \theta=\theta_0(z)\end{aligned}\right\},$$

where V_e is a constant and $\theta_0(z)$ is prescribed. These conditions are not all independent.

The numerical method differs from that used in TG; here the equations are integrated in their primitive form. The techniques are standard but a few details are given in an appendix. The calculations are commenced from the initially quiescent state $(u,v,w)=(0,0,0)$, $\theta=\theta_0(z)$, with the body force applied impulsively at the initial instant $t=0$, and terminated when a steady state is attained.

3. Parameter values

The parameter values taken in the present calculations are mostly the same as those used in TG and are broadly appropriate to the atmospheric situation. Thus, we take $R=2$ km, $H=3$ km, $V_e=2.5$ m s^{-1} (corresponding with a circulation $\Gamma=2\pi RV_e$ equal to 3.1×10^4 m s^{-1} and a mean vertical vorticity $\Gamma/\pi R^2$ equal to 2.5×10^{-3} s^{-1}), $K_M=K_H=10$ m s^{-1}, giving a *pseudo-Reynolds number* $\Gamma/K_M=3.1\times10^3$, $g=9.8$ m s^{-2} and $c_p=1005$ J kg^{-1} K^{-1}. The body force has a magnitude of 2.4 m s^{-2} on the axis,[1] tapering linearly

[1] See TG for a fuller discussion of this choice.

TABLE 1. Static stability in the numerical experiments.

Experiment	$\theta_0(z)$
1	$\equiv 300$
2	$=300+\mu z$, $\mu=3$ K km^{-1}
3	$=300+\mu z$, $\mu=4$ K km^{-1}
4	$=300+\mu z$, $\mu=5$ K km^{-1}
5	$=\begin{cases}300+\mu_1 z, & \mu_1=6 \text{ K km}^{-1}, \quad 0\leqslant z\leqslant 1 \text{ km} \\ 306+\mu_2(z-1), & \mu_2=3 \text{ K km}^{-1}, \quad 1\leqslant z\leqslant 3 \text{ km}\end{cases}$

TABLE 2. Specification of experiments 6, 7 and 8.

Experiment	Specification
6	as in Experiment 5 but with $K_H=2$ m^2 s^{-1}
7	as in Experiment 1 but with $H=4.5$ km and the lower end of the body force at 2.5 km
8	as in Experiment 7 with $\theta_0(z)$ as in Experiment 5 and continuing to increase at the rate 3 K km^{-1} up to $z=H$

to zero at two radial grid lengths from the axis, and its lower end at a height of 1.5 km.

The first five experiments described below differ only in the choice of $\theta_0(z)$ as specified in Table 1. Three further experiments also discussed are defined in Table 2.

4. Results and discussion

The streamlines and isotachs of swirling velocity for experiments 1, 3, 4 and 5, and the isentropic surfaces for experiments 3, 4, 5 and 6, when the flows have become steady, are shown in Figs. 2, 3 and 4, respectively. In addition, some data obtained from the eight calculations in the steady state are listed in Table 3, including the following:

- $w_{\max}$ maximum vertical velocity
- $v_{\max}$ maximum swirling velocity
- $r_{\max}$ radius at which $v_{\max}$ occurs
- Δp maximum pressure reduction across the vortex
- A amplification factor, defined as $(v_{\max}/r_{\max})/(V_e/R)$, a measure of the angular rate of rotation of the vortex compared with that of the ambient field of rotation
- T_F time taken to reach a steady state, based on the arbitrary criterion that the total kinetic energy changes by less than 1% over ten time steps. In cases where a vortex develops to the lower boundary, it does so in a time which is approximately 0.85 T_F.

Table 3 also includes the corresponding data for experiment 4 in TG, the homogeneous flow version of experiment 1 here.

A comparison of parts (a), (b) and (c) of Figs. 2 and 3 and reference to Table 3 shows that as the static stability is increased, the strengths of the meridional circulation and of the vortical flow are reduced; the vortex core increases in width and the surface inflow layer progressively deepens so that when $d\theta_0/dz = 5$ K km^{-1}, one would judge that the vortex no longer interacts strongly with the ground in a shallow friction layer,[2] but terminates aloft. These effects are as expected, for an increase in vertical stability inhibits the vertical motion, leading to reduced radial convergence or equivalently to weaker radial pressure gradients. As a consequence, for the same imposed circulation Γ, cyclostrophic balance aloft is achieved at larger radii, thereby reducing local swirling velocities and increasing the vortex width. Nevertheless, the calculations must be performed to determine the extent of these changes.

It is perhaps also interesting to note that when compared with the corresponding homogeneous vortex studies in TG, the extra realism gained here by including the effect of decreasing density with height on the inertia of air leads, in the absence of stability, to a small increase in the vortex strength—again as expected.

Since an increase of potential temperature with height of 5 K km^{-1} over a depth of 3 km or more appears unrealistically large (compare an average rate of slightly more than 3 K km^{-1} for the U.S. Standard Atmosphere below 3 km), we were led to carry out experiment 5, in which an increase of 6 K km^{-1} occurs in the lowest kilometer (a value suggested as typical by Goff's data) and only 3 K km^{-1} above this height; the aim being to assess the effect of stronger stability in a shallow layer near the ground. However, a comparison of experiments 4 and 5 [cf. parts (c) and (d) of Figs. 2 and 3 and the relevant data in Table 4] shows only minor differences between these two flows, both in strength and structure.

Figs. 4a–4c reveal a slight dip in the isentropic surfaces at larger radii caused by the downward advection of potentially warm air by the meridional circulation, whereas air in the vortex core is markedly colder than ambient air at the same level due to the forced ascent of potentially cold air from lower levels.

TABLE 3. Steady-state flow data. See text for details.

Experiment	$r_{\max}$ (m)	$v_{\max}$ (m s^{-1})	$w_{\max}$ (m s^{-1})	Δp (mb)	A	T_F (min)
4 in TG	38	70	77	59	1470	4½
1	38	73	80	60	1520	4½
2	41	60	69	49	1160	4¾
3	48	53	56	33	890	5
4	52	49	51	29	760	4¾
5	51	50	53	30	790	4¾
6	51	58	63	33	900	4¼
7	38	78	88	62	1640	17
8	52	54	59	32	830	14½

[2] For a detailed discussion of surface friction effects, the reader is referred to Bode *et al.* (1975).

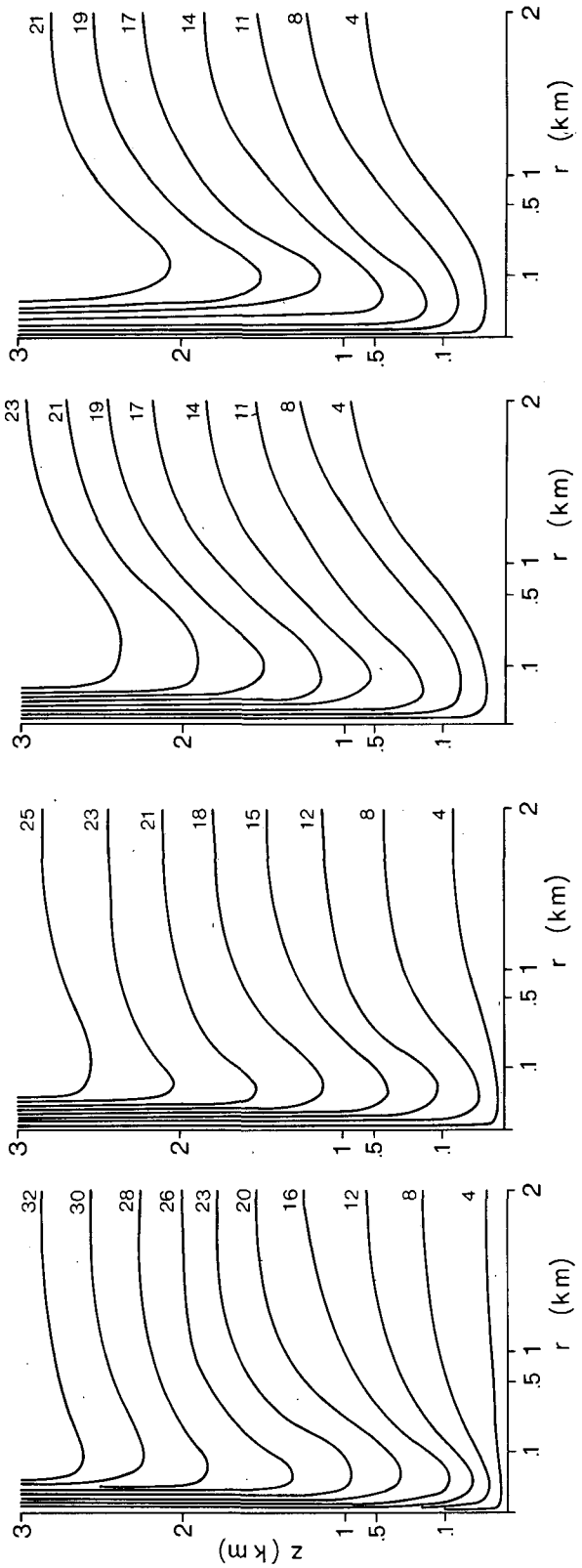

FIG. 2.

FIG. 3.

FIG. 2. Comparison of steady-state streamlines: (a) experiment 1, (b) experiment 3, (c) experiment 4, (d) experiment 5. Units labeling the isopleths are in 10^6 m^2 s^{-1}. In this figure, the coordinates have been stretched logarithmically in the L-shaped region $0 \leqslant r \leqslant 1$ km and $0 \leqslant z \leqslant 1$ km to overcome bunching of contours near the axis and near the surface.

FIG. 3. Comparison of steady-state isotachs of swirling velocity: (a) experiment 1, (b) experiment 3, (c) experiment 4, (d) experiment 5. Units labeling selected contours are in m s^{-1}. The coordinates are stretched as in Fig. 2.

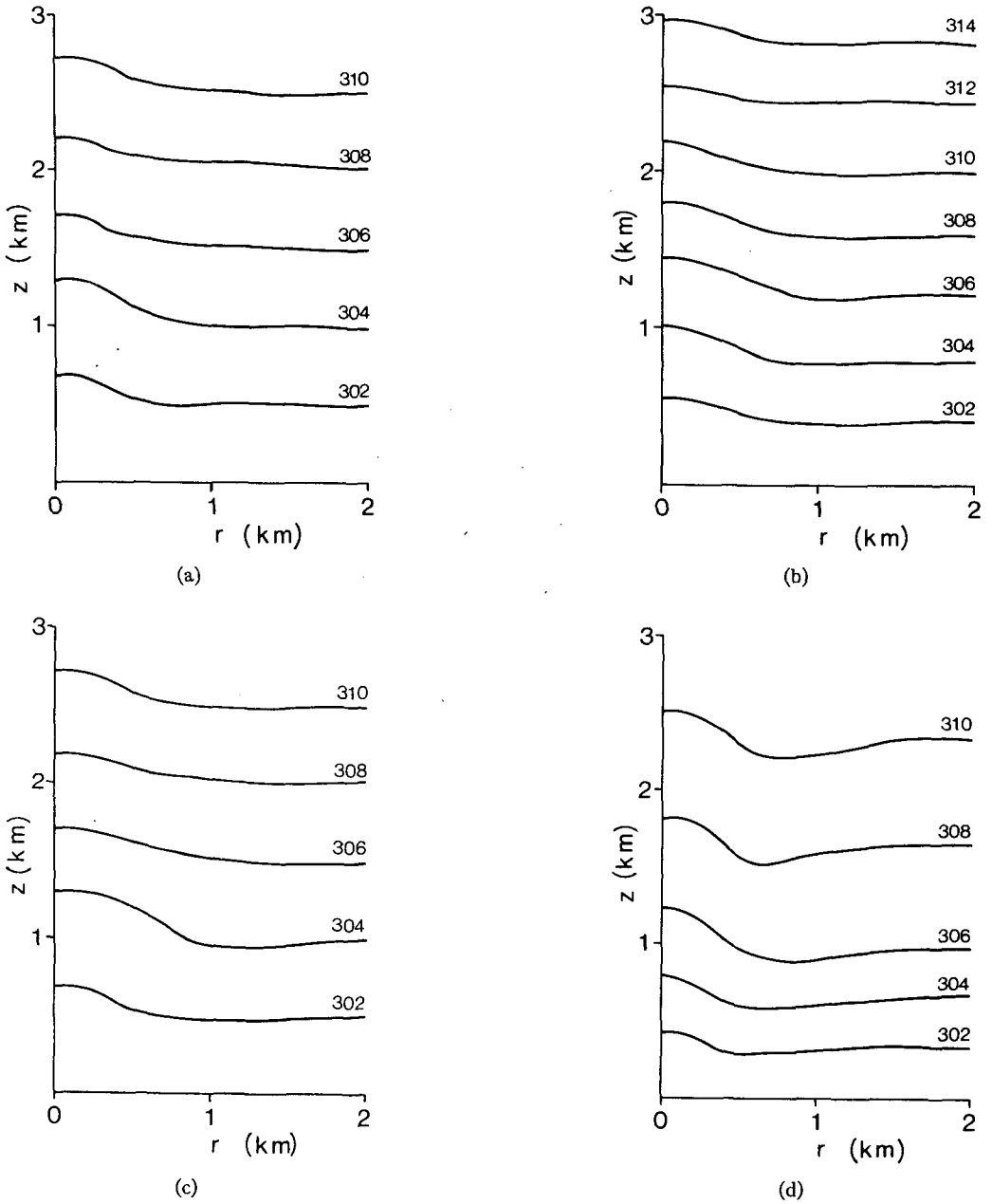

FIG. 4. Comparison of steady-state isentropes (K): (a) experiment 3, (b) experiment 4, (c) experiment 5, (d) experiment 6. The coordinates are unstretched.

It is evident that thermal diffusion is considerable in these experiments and K_H, like K_M, is probably at least an order of magnitude too large outside the vortex and also in parts of the vortex itself, especially where the flow is most stably stratified with respect to density and/or rotation. However, in the absence of data on diffusivity distributions in the tornado environment, and in view of the excessive amount of computer time which would be required to explore this facet of the problem in depth, we have indulged ourselves in only one additional calculation—experiment 6—by repeating experiment 5 with K_H reduced by a factor of 5 and K_M held fixed. As anticipated, the isentropes in experiment 6 have a more pronounced dip at larger radii (Fig. 4d) reflecting the increased importance of advection over diffusion, and the core temperature is slightly warmer at each level, presumably because air which descends outside the vortex loses less heat by diffusion toward the ground and is therefore warmer when it reascends in the vortex core. Apparently, the warmer core allows both the meridional circulation and the swirling flow

TABLE 4. Ratio Λ of buoyancy force to axial dynamic pressure gradient force at selected heights on the vortex axis in experiment 5.

z (km)	0.25	0.5	0.75	1.0	1.25	1.5
Λ	−0.49	−0.40	−0.33	−0.27	−0.19	−0.10

to develop a little more strongly than in experiment 5 (see Table 4). Undoubtedly, these effects will become more pronounced as K_H decreases further.

The importance of the cold core on the dynamics of the vortices described above may be estimated using Table 4, which gives the computed ratio Λ, of buoyancy force B to the local, axial, dynamic pressure gradient at selected levels on the vortex axis in experiment 5. Here B is defined in the usual way[3] as $g(\rho_0-\rho)/\rho$ and the dynamic pressure gradient is[4] $-\rho^{-1}\partial p'/\partial z$, where $p'=p-p_0$, ρ is the local air density and p_0 and ρ_0 are the ambient pressure and density, respectively, at the same level. In terms of the ambient potential temperature and Exner function, the ratio Λ takes the form

$$\Lambda=\frac{B}{-\rho^{-1}(\partial p'/\partial z)}=\frac{g(\theta'/\theta_0)+W}{-c_p\theta(\partial\pi'/\partial z)-W}, \tag{4.1}$$

where

$$W=g\frac{\theta}{\theta_0}\left[\left(\frac{\pi}{\pi_0}\right)^{1-(1/\kappa)}-1\right]. \tag{4.2}$$

Thus, in this experiment, the negative buoyancy is as much as one-half the axial pressure gradient at low levels, but decreases in relative importance with height and becomes small in the neighborhood of the forcing region. Of course, these ratios will be smaller when the vertical stability is less.

Since there have been no measurements of thermal structure in tornadoes, any attempt to assess the relevance of the foregoing results must inevitably involve some degree of speculation, but an important purpose of the calculations is to educe the various factors which determine the thermal structure. First, we note that besides horizontal temperature differences, there are two other effects which contribute to the buoyancy field of a tornado. These are the latent heat release due to the condensation of water vapor in the funnel cloud (and possibly that consumed by the evaporation of cloud droplets near the edge of this cloud) and the reduction of density in the core due to the reduction of pressure there. It is difficult to assess the importance of latent heating effects in the context of the present model and these are currently under study by the authors. Even so, there is reason to believe that these are not crucially important (see, e.g., Morton, 1966, p. 163). The buoyancy effect of reduced density in the core is represented by the term W in the expression for B and is included in our calculations in the term $-c_p\theta\partial\pi'/\partial z$, which is equal to $-\rho^{-1}\partial p'/\partial z+W$. The dynamical importance of this effect can be gauged from Table 5, which lists the values of Λ at a series of levels on the axis in experiment 1. In this experiment, the potential temperature is everywhere uniform and any buoyancy forces are due solely to W. It can be seen that for this vortex, the strongest hitherto described, the ratio may be regarded as appreciable at levels where the vortex is most intense.

TABLE 5. Ratio Λ of buoyancy force W to axial dynamic pressure gradient force calculated at selected heights on the vortex axis in experiment 1.

z (km)	0.25	0.5	0.75	1.0	1.25	1.5
Λ	0.11	0.13	0.15	0.18	0.20	0.20

In an early review paper on severe storms Ludlam (1963, p. 24) argues that "at least a proportion of the air which ascends in the tornado must be derived from the cold outflow; if this contains the potentially cold air from middle levels its ascent might be expected soon to impede if not destroy the tornado." He goes on to suggest that "it may be particularly important for the intensification and persistence of a tornado that some of the downdraft air may be derived from potentially warm air which enters the left flank of the storm at low levels." Our calculations give broad support to these ideas and suggest that observed levels of vertical stability may indeed be sufficient to inhibit tornado-genesis in some situations. However, if vertical forcing is sufficiently intense that a strong tornado becomes established, it is conceivable that the meridional circulation which it induces might be sufficient to cause a local disruption of the cold surface layer by advecting the warm moist air which feeds the updraft to low levels in the vicinity of the vortex. This possibility is excluded in the present model by the specification of $\theta(R,z)$ at the radial boundary and $\partial\theta/\partial z=0$ on the entire upper boundary. However it would presumably occur with the alternative boundary condition $\partial\theta(R,z)/\partial r=0$ on the whole radial boundary, providing that the aspect ratio R/H is sufficiently large and the stratification sufficiently weak for areas of subsidence to be induced through the upper boundary. It would also be necessary to specify $\theta(r,H)$ instead of $\partial\theta/\partial z$ for subsiding air.[5]

[3] The reader is reminded that the definition of buoyancy force depends on the arbitrary subdivision of the total pressure into a local reference pressure and a dynamic pressure. The reference pressure is usually taken to be the ambient hydrostatic pressure distribution, but other choices are possible and lead to different distributions of "buoyancy force" (see e.g., Smith *et al.*, 1975, pp. 9–12).

[4] In this formula, pressure must, of course, be taken in SI units.

[5] Note: if $\partial\theta(R,z)/\partial r=0$ for $0\leqslant z\leqslant H$, the value of $\theta(R,z)$ is determined as part of the solution. With $\partial\theta(r,H)/\partial z$ taken also as zero for $0\leqslant r\leqslant R$, the ground would serve as the only heat source or sink and one would anticipate that θ would become uniform, equal to $\theta_0(0)$, as the flow attained the steady state.

These latter conditions are suggested by the detailed comparison of alternative thermal conditions given by Smith *et al.* (1975) in the context of convection produced by a localized heat source at the ground.

An appraisal of our model vortices would be incomplete without giving consideration to the possible geometrical constraint implied by a particular choice of computational domain size. The consequences of changing the radial extent of the computational region when the ambient circulation is held fixed are explored by Leslie and Smith (1977) in a simulation of dust devils and those results are relevant here. Basically an increase in R leads to a reduction of vortex intensity and an increase in core width, due mainly (at least at high pseudo-Reynolds number) to the additional frictional stresses at the lower boundary on account of its larger area. These effects are unavoidable and must be borne in mind when comparing the results of numerical simulations of flows in finite regions with their unbounded atmospheric counterparts. The consequences of extending the height of the computational region cannot be deduced from the forementioned paper as the vortices therein are driven thermally from below and an increase in H does not alter the gross driving strength. In the present model, however, the total driving strength depends on the vertical extent of the forcing region and to achieve true comparability, we would need to increase H keeping fixed the vertical distribution of the body force. It seems more interesting and more realistic to change both of these and accordingly we have carried out experiments 7 and 8 in which H is increased to 4.5 km and the body force is held fixed in magnitude but is applied only above 2.5 km. In experiment 7 the potential temperature is uniform and there are no buoyancy forces, whereas in experiment 8 the ambient potential temperature increases linearly at rates of 6 K km^{-1} and 3 K km^{-1} below and above a height of 1 km as in experiment 5. As a result of these changes, the vortices in experiments 7 and 8 are slightly stronger than their respective counterparts in experiments 1 and 5 and take appreciably longer to form (Table 3). Indeed, their growth times are more in line with those for the development of tornado vortex signatures (typically 30 min) from cloud midlevels to the ground, as revealed by Doppler radar observations. The difference in vortex strength between experiments 7 and 8 is also comparable with the corresponding difference between experiments 1 and 5, but the effect of stable stratification on the downward penetration of the vortex is more promient when the body force is raised to a higher level. This can be seen in Fig. 5 which shows the isotachs of swirling velocity for experiments 7 and 8. The vortex in experiment 8 unmistakably terminates aloft (cf. Figs. 5b and 4d) whereas in the absence of stability, the mature vortex has an extensive core of high swirling velocity, ending in a shallow friction layer at the ground.

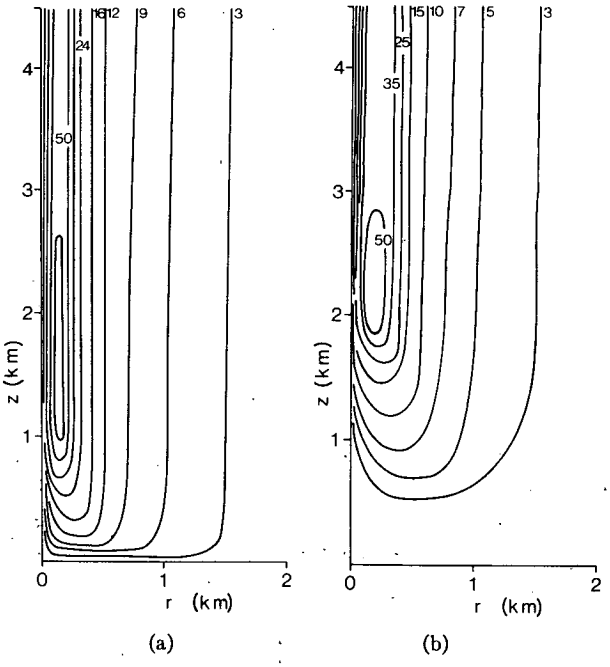

FIG. 5. Comparison of steady-state isotachs of swirling velocity in experiments 7 and 8 for (a) neutral stratification, vortex extends to the ground; and (b) stable stratification, vortex terminates aloft. Units labelling selected contours are in m s^{-1}. The coordinates are stretched as in Fig. 2.

5. Conclusions

We have extended the model for tornadogenesis in TG to an adiabatic atmosphere and to one in which the tornado environment is stably stratified at low and intermediate levels. Despite its limitations, the model accounts for many of the observed aspects of tornadogenesis and reveals the salient dynamical processes and constraints which appear to be involved.

We have demonstrated here the likely importance of static stability as a factor opposing tornadogenesis and have shown that this may cause some vortices to terminate aloft. Such vortices would appear as rotating, pendant funnel clouds if they extended below cloud base.

Our results show also that the buoyancy effect due to the reduced pressure, and therefore density, in the vortex core may contribute significantly to the force balance within the core.

Finally, with the more realistic domain size and vertical distribution of body force, the growth times of the simulated vortices in experiments 7 and 8 are comparable with the times taken for tornado vortex signatures, revealed by Doppler radar, to extend from cloud midlevels to the ground.

Acknowledgment. We are grateful to Keith Stewartson of University College, London, who, on a recent visit to Monash University, listened intently to the ideas presented here and offered many constructive

comments. It was a result of these discussions which led us to carry out experiments 7 and 8. We are grateful also to Bob Davies-Jones at NSSL for a number of comments on the original version of this manuscript.

APPENDIX

Numerical Procedure

Eqs. (2.1)–(2.5) may be written as

$$\frac{\partial}{\partial r}(\rho_0 r u)+\frac{\partial}{\partial z}(\rho_0 r w)=0, \tag{A1}$$

$$\frac{\partial u}{\partial t}=-c_p\theta\frac{\partial \pi'}{\partial r}+N_u+D_u, \tag{A2}$$

$$\frac{\partial v}{\partial t}=N_v+D_v, \tag{A3}$$

$$\frac{\partial w}{\partial t}=-c_p\theta\frac{\partial \pi'}{\partial z}+F+\frac{g\theta'}{\theta_0}+N_w+D_w, \tag{A4}$$

$$\frac{\partial \theta}{\partial t}=N_\theta+D_\theta, \tag{A5}$$

where N_u, N_v, N_w, N_θ are the various advective and curvature terms and D_u, D_v, D_w, D_θ are diffusive terms. The four prognostic equations (A2)–(A5) are solved explicitly using central time and space differencing on a staggered grid in the manner described by Williams (1969) and later employed by Eskridge and Das (1976). Having obtained the updated values of u, v, w and θ, it remains to solve for π'; this is achieved by eliminating the $\partial u/\partial t$ and $\partial w/\partial t$ terms from (A2) and (A4) by combining them with (A1). The resulting equation for π' is

$$\frac{\partial^2\pi'}{\partial r^2}+\frac{\partial^2\pi'}{\partial z^2}+\frac{\partial}{\partial r}[\ln(\rho_0 r\theta)]\frac{\partial \pi'}{\partial r}+\frac{\partial}{\partial z}[\ln(\rho_0 r\theta)]\frac{\partial \pi'}{\partial z}$$
$$=\frac{1}{\rho_0 r\theta}\left[g\frac{\partial}{\partial z}\left(\rho_0 r\frac{\theta'}{\theta_0}\right)+\frac{\partial}{\partial z}(\rho_0 rF)+\frac{\partial}{\partial r}(\rho_0 rN_u)+\frac{\partial}{\partial z}(\rho_0 rN_w)\right.$$
$$\left.+\frac{\partial}{\partial r}(\rho_0 rD_u)+\frac{\partial}{\partial z}(\rho_0 rD_w)\right]. \tag{A6}$$

Eq. (A6) is readily solved by successive overrelaxation techniques, and all the dependent variables have then been calculated. The complete cycle of solving (A2)–(A6) is repeated until the desired number of time steps has been reached.

In experiments 1–6, the finite-difference mesh has 121 points in the vertical and 81 in the horizontal, corresponding with a grid spacing of 25 m; an integration time step of 0.25 s is used. In experiments 7 and 8, extra grid points are used in the vertical to maintain the grid spacing of 25 m. The calculations were performed on the CSIRO Cyber 76 computer in Canberra.

REFERENCES

Bode, L., L. M. Leslie and R. K. Smith, 1975: A numerical study of boundary effects on concentrated vortices with application to tornadoes and waterspouts. *Quart. J. Roy. Meteor. Soc.*, **101**, 313–324.

Brandes, E. A., 1977a: Flow in severe thunderstorms observed by dual-doppler radar. *Mon. Wea. Rev.*, **105**, 113–120.

——, 1977b: Mesocyclone evolution and tornado generation within the Harrah, Oklahoma storm. NOAA Tech. Memo. ERL NSSL-81, 28 pp.

Brown, R. A., and L. R. Lemon, 1976: Single doppler radar vortex recognition: Part II—tornadic vortex signatures. *Preprints 17th Conf. Radar Meteorology*, Seattle, Amer. Meteor. Soc. 104–109.

Burgess, D. W., 1976: Single doppler radar vortex recognition: Part 1—Mesocyclone signatures. *Preprints 17th Conf. Radar Meteorology*, Seattle, Amer. Meteor. Soc., 97–103.

Eskridge, R. E., and P. Das, 1976: Effect of a precipitation-driven downdraft on a rotating wind field: A possible trigger mechanism for tornadoes? *J. Atmos. Sci.*, **33**, 70–84.

Goff, R. C., 1976: Vertical structure of thunderstorm outflows. *Mon. Wea. Rev.*, **104**, 1429–1440.

Leslie, L. M., and R. K. Smith, 1977: On the choice of radial boundary conditions for numerical models of sub-synoptic vortex flows in the atmosphere with application to dust devils. *Quart. J. Roy. Meteor. Soc.*, **103**, 499–510.

Ludlam, F. H., 1963: *Severe Local Storms: A review. Meteor. Monogr.*, No. 27, 1–30.

Morton, B. R., 1966: Geophysical vortices. *Progress in Aeronautical Science*, Vol. 7, D. Küchemann, Ed., Pergamon, 145–194.

——, 1969: The strength of vortex and swirling core flows. *J. Fluid Mech.*, **38**, 315–333.

Ogura, Y., and N. A. Phillips, 1962: Scale analysis of deep and shallow convection in the atmosphere. *J. Atmos. Sci.*, **19**, 173–179.

Smith, R. K., and L. M. Leslie, 1978: Tornadogenesis. *Quart. J. Roy. Meteor. Soc.*, **104**, 189–199.

——, B. R. Morton and L. M. Leslie, 1975: The role of dynamic pressure in generating fire wind. *J. Fluid Mech.*, **68**, 1–19.

Williams, G. P., 1969: Numerical integration of the three-dimensional Navier-Stokes equations for incompressible flow. *J. Fluid Mech.*, **37**, 727–750.